DYNAMIC RESPONSE ANALYSIS OF WIND TURBINE TUBULAR TOWERS UNDER LONG-PERIOD GROUND MOTIONS WITH THE CONSIDERATION OF SOIL-STRUCTURE INTERACTION

Tao Huo[1,2], Lewei Tong[1, 2,*] and Yunfeng Zhang[2, 3]

[1]*State Key Laboratory of Disaster Reduction in Civil engineering , Tongji University，Shanghai, 200092, China*
[2]*College of Civil Engineering, Tongji University, Shanghai 200092, China*
[3]*Department of Civil & Environmental Engineering, University of Maryland, College Park, MD 20742, US*
** (Corresponding author: E-mail: tonglw@tongji.edu.cn)*

Received: 13 July 2016; Revised: 24 May 2017; Accepted: 25 June 2017

ABSTRACT: Existing research in the seismic response of wind turbine tubular towers subjected to long-period ground motions is lacking, especially when soil-structure interaction (SSI) is considered. This paper discusses the seismic performance of typical pitch-controlled 1.25MW wind turbine systems, with particular focus on the influences of SSI effect and ground-motion characteristics. Modal analysis and resonance analysis are carried out first, ensuring that resonance does not occur when the tower is in operation. Two long-period waves and a bedrock wave are selected from the worldwide earthquake record database, followed by detailed dynamic time history analysis. The results indicate that the maximum displacement, acceleration, stress level and internal force responses of the tower subjected to the long-period ground motions are significantly larger than the corresponding values induced by the bedrock wave. Some responses can be further amplified due to the SSI effect, and this highlights the importance of incorporating the SSI effect into seismic design of wind turbine towers, especially for those located in soft soil regions. Furthermore, neglecting the vertical seismic action could lead to unsafe design. Other important issues, including the risk of pounding, stress concentration near the door regions, spindle shear fracture, and foundation failure, are also discussed, and summarized as references or comments for design and analysis of such structures.

Keywords: Soil-structure interaction (SSI), Long-period ground motion, Wind turbine tubular towers, Time history analysis, Design and analysis comments

DOI: 10.18057/IJASC.2018.14.2.6

1. INTRODUCTION

Since the 20th century, traditional energy source has been exhaustingly consumed, leading to global energy crisis. After the 1970s, the concept of sustainable energy became prevalent, and wind power, which is a renewable source of energy, has been extensively developed [1]. Modern commercial wind turbine system originated in Northern Europe which is not a seismically active region; therefore engineers were more concerned about the wind-induced dynamic response at that time. However, with an increasing number of wind turbine systems being constructed in the seismically active region all over the world [2], it is essential to revisit the dynamic performance of these systems against seismic action.

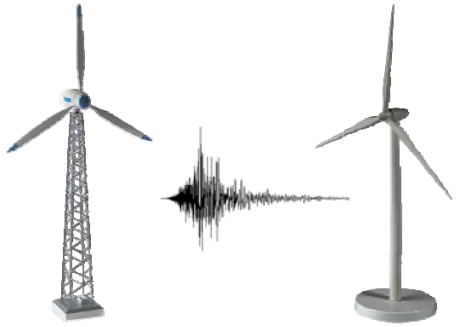

Figure 1 Typical Wind Turbine Lattice Tower and Wind Turbine Tubular Tower

There are two common types of the horizontal-axis wind turbine towers, namely, lattice tower and tubular tower, as shown in Figure 1 [2, 3]. Lattice towers, which are widely used in small and medium-sized wind turbine systems, have their merits of low cost and convenient transportation, but turbulence issues for blade along the downwind direction may be caused. On the other hand, tubular towers have the advantages of elegant appearance, good vibration performance, and convenient maintenance. Therefore, tubular towers, which are the focus of the current study, are widely employed in large-scale wind turbine systems [2].

Some researchers have conducted a series of modeling and dynamic analysis on wind turbine tubular towers. Lobitz [4] proposed a mass-damping-spring model for wind turbine towers and carried out dynamic time history wind analysis; however, no seismic analysis was conducted. Through using mass-damping-spring model in seismic dynamic time history analysis, Bazeos et al. [5] found that the soil-structure interaction (SSI) effect has a significant influence on the dynamic response of tubular towers. Lavasas et al. [6] presented a finite element model containing both the tubular tower and the foundation, where the SSI effect was considered through introducing contact elements. However, in that study, only static analysis was performed without considering any dynamic effects. It is noted that in their studies [5, 6], the blades and nacelle were not directly built in the models. Witcher [7] used both time domain and response spectrum methods to study the seismic response of a 2 MW wind turbine tower. The results showed that the time domain method is more accurate. Based on a shear transfer mechanism, Murtagh et al. [8, 9] developed a coupling finite element model for connecting the tower and blades. The coupling mechanism was defined in detail and dynamic time history analysis was conducted to investigate the wind load effect. Taking SSI effect into account through introducing springs and dampers, Zhao and Maißer [10,11] established multi-body dynamic models for the wind turbine towers to investigate the seismic behavior in time domain and confirmed that the SSI effect plays more significant roles in higher mode vibrations. Through adopting a combined modal and multi-body dynamic formulation, Prowell et al. [12] examined the seismic behavior of a typical 5MW wind turbine system and concluded that the bending vibrations of the towers induced by earthquake loading need to receive sufficient attention in the design. Díaz et al. [13] presented an analytical model of an operating wind turbine subjected to three components base accelerations. The results indicated that in strong earthquake regions, the wind turbine design, especially the tubular tower section, can be controlled by the combined action of the earthquake and wind load. Based on a simplified soil spring model and Boundary Element Method, Taddei et al. [14] established a simplified finite element model of wind turbine towers and adopted a spectrum-compatible synthetic acceleration method to evaluate the applicability of the simplified soil representation in the practical seismic design. The results showed that with increasing thickness of the soil layer, their natural frequencies decrease, and the simplified soil spring model could have better agreement with more sophisticated and accurate soil models. Alati et al. [15] inveatigated the seismic behaviour of fully coupled offshore wind turbine models with fixed and flexible foundations under some typical load cases, and it was concluded that the fully coupled models can provide better prediction on the dynamic responses of the blades,

which are more sensitive to the foundation flexibility. More recently, some innovative vibration reduction solutions, adoping smart materials such as shape memory alloys [16, 17], were also proposed for wind turbine towers[18, 19].

While continuous progress has been made looking into the seismic performance of wind turbine towers, relevant investigations on the influences of long-period ground motions and the SSI effect are generally lacking. Far field, long-period seismic ground motions could bring serious damage to flexible structures [20]. So far, long-period ground motion characteristics and response spectrums have been investigated by various researchers [21, 22], with the main focus on high-rise buildings [23, 24]. However, relevant studies on wind turbine tubular towers subjected to long-period ground motions are still insufficient, and in addition, the long-period range of the response spectrum in major codes [25,26] may not fully meet the design requirement for long-period structures including wind turbine systems. Pounding between the blades and the tower under certain circumstances can be another issue which needs to be carefully addressed. Therefore, it is necessary to take an in-depth look into the seismic response of wind turbine tubular towers subjected to long-period ground motions, taking the SSI effect into account.

In light of the above, a detailed finite element model, consisting of rotor, nacelle, tower and foundation, is established and discussed in this study. The study starts with the introduction of the prototype wind turbine system and the modeling strategy, followed by the discussions of modal analysis and resonance analysis results. A set of dynamic time history analysis are then conducted, where different types of seismic ground motions are considered and the structural responses under long-period seismic ground motions (waves) and bedrock seismic ground motion (wave) are discussed in detail. Based on the numerical results, some preliminary design and analysis recommendations are finally made.

2. INTEGRATED FINITE ELEMENT MODEL

2.1 Description of Prototype Wind Turbine System

This study considers a typical pitch-controlled 1.25MW wind turbine system, based on which an integrated finite element model was built. The key material properties of the blade, nacelle and tower body are listed in Table 1. In the current study, the material was assumed to remain elastic under the considered design earthquakes; in other words, only elastic time-history analysis was performed for the tower. In addition, the three blades were simplified as cantilever beams with a rectangular cross section. The length, width and depth of each blade are 32.175m, 1.5m and 0.3m, respectively. The mass of the rotor (including the blades and hub) is 27470kg. The nacelle and its internal components were treated as an integrated part in the model. The length, width and height of the nacelle are 9.8m, 3.22m and 3.01m, respectively. The mass of the whole nacelle is 52000kg. The main body of the tower is comprised of three segments with varying cross section properties, and the height of each segment is 10.14m, 21.486m and 30.211m (from bottom to top), making a total height of 61.837m. The corresponding tube wall thicknesses for the three segments are 20mm, 16mm and 12mm, respectively. The diameter of the tower increases linearly from 4.2m at the bottom to 2.58m at the top. In order to facilitate maintenance and testing, a door is opened near the bottom of the tower. The height and width of the door is 1.8m and 0.8m respectively in the vertical projection plane. In order to avoid local shell buckling, a doorframe is also installed, as shown in Figure 2b. A 10m×10m×1.8m reinforced concrete raft foundation is located at the bottom of the tower, and the yaw angle of the tower is 0 degree. As defined in Figure 2a, the blades rotational plane is perpendicular to X-Direction, the direction along the tower height is labeled as Z-axis, and the location where the blade is parallel to the positive direction of Z-axis is defined as 0^o azimuth

angle. Murtagh et al. [9] observed that the most unfavourable location of the blades is 0°. In addition, Alati et al. [15] found that the influences of different spatial positions of the blades on the seismic responses are not notable. Therefore, this study only considers the critical location (0°) of the blades to investigate the seismic performance of wind turbine systems, as shown in Figure 2a.

Table 1. Material Properties of Structural Components used in ANSYS

Components	Material	Modulus of elasticity (GPa)	Poisson's ratio
Blade	Glass Reinforced Plastic	42.60	0.22
Nacelle	Steel(Q345D)	206	0.30
Tower	Steel(Q345D)	206	0.30

(a) Integrated finite element model (b) Doorframe

Figure 2. Integrated Finite Element Model and Doorframe

2.2 Modeling

Using the commercial software ANSYS [27], an integrated finite element model was established (see Figure 2a). Eight-node shell elements (SHELL181) were adopted to model both the blades and the tower. The nacelle including inner components was simulated by beam elements (BEAM 189). Following the GL Guideline [28], solid elements (SOLID 95) were used to simulate the doorframe. The foundation section was modeled using reinforced concrete solid elements (SOLID 65). Due to the differences of element types and mesh densities among components, constraint equations and coupling interactions were applied to connect different types of elements. In particular, Rigid Zone connections using the CERIG command were employed between the tower top circular nodes and nacelle beam nodes. Rigid Zone connections were also used between the central nodes of the three blades and the end nodes of the nacelle beam, as shown in Figure 3a. Apart from that, coupling interactions were utilized between the tubular tower nodes along the thick direction and the doorframe nodes through the CPINTF command (see Figure 3b). Constraint equation connections were applied between the tower bottom circular nodes and the foundation top nodes using the CEINTF command (see Figure 3c).

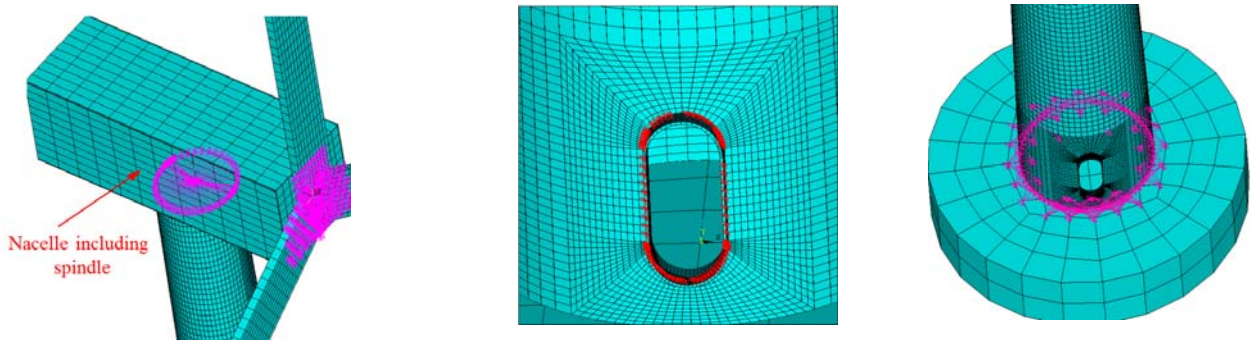

(a) Rigid Zone connection

(b) Coupling connection between tubular tower and doorframe

(c) Constraint equation connection between tubular tower and foundation

Figure 3. Constraint Equations and Coupling Interactions between Different Types of Elements

In order to examine the influence of the SSI effect on the dynamic behavior of the wind turbine system, two models were compared in this study: one model taking account of the SSI effect and the other one excluding this effect. Wolf [29] and Richart et al. [30] suggested that the influence of SSI effect on structural dynamic performance could be achieved by introducing a series of discrete springs and dampers between the soil and the foundation. Using this strategy, a series of discrete springs and dampers were incorporated into the soil-foundation interface. Elements COMBIN14 were applied to simulate the interaction between the foundation and soil in ANSYS. The details of the mechanical model considering the SSI effect are shown in Figure 4, and the values of the foundation soil parameters are provided in Table 2.

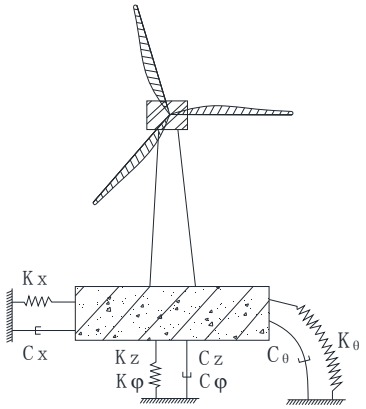

Figure 4. Mechanical Model Considering SSI Effect

Table 2. Parameters of Foundation Soil

Density (Kg/m^3)	Cohesive stress (Pa)	Poisson's ratio	Shear modulus (Pa)	Shear wave velocity (m/s)	Internal friction angle (°)	Dilatancy angle (°)
1900	19000	0.333	5.60E+06	150	25	29

As can be seen in Figure 4, the soil-structure interaction can be modeled with two-dimensional soil spring stiffness coefficients, damping coefficients and mass of springs [29-32]. The basic properties of the springs and dampers were determined from the following equations[29, 30]:

$$K_x = K_y = \frac{8G_sR_s}{2-\nu_s} \qquad K_z = \frac{4G_sR_s}{1-\nu_s} \qquad K_\theta = \frac{8G_sR_s^3}{3(1-\nu_s)} \qquad K_\varphi = \frac{16}{3}G_sR_s^3 \tag{1}$$

$$C_x = C_y = \frac{4.6R_s^2}{2-\nu_s}\sqrt{G_s\rho_s} \quad C_z = \frac{3.4R_s^2}{1-\nu_s}\sqrt{G_s\rho_s} \quad C_\theta = \frac{0.745R_s^4}{1-\nu_s}\sqrt{G_s\rho_s} \quad C_\varphi = 0.815R_s^4\sqrt{G_s\rho_s} \tag{2}$$

$$M_x = M_y = \frac{0.76\rho_s R_s^3}{2-\nu_s} \quad M_z = \frac{1.08\rho_s R_s^3}{1-\nu_s} \quad M_\theta = \frac{0.64\rho_s R_s^5}{(1-\nu_s)} \quad M_\varphi = 0.24\rho_s R_s^5 \tag{3}$$

Where K_x and K_y are the horizontal stiffness coefficients; K_z is the vertical stiffness coefficient; K_θ is the rotational stiffness coefficient; K_φ is the torsional stiffness coefficient. Similarly, $C_i, M_i (i = x, y, z, \theta, \varphi)$ are the corresponding damping coefficients and mass of springs, respectively; R_s is the radius of the circular foundation; G_s, ν_s and ρ_s are the shear modulus, Poisson ratio and density of the soil, respectively.

Substituting the considered soil parameters given in Table 2 into Eq. 1 through Eq. 3, the spring and damper parameters used in ANSYS are calculated and given in Table 3.

Table 3. Property of Springs and Dampers

Directions of degree of freedom	Stiffness coefficients	Damping coefficients	Mass of springs
Horizontal direction	1.34E+08 N/m	7.12E+06 N·s/m	1.08E+05 Kg
Vertical direction	1.68E+08 N/m	1.31E+07 N·s/m	3.85E+05 Kg
Rotational direction	2.80E+09 N·m	7.20E+07 N·s·m	5.70E+06 Kg·m^2
Torsional direction	3.73E+09 N·m	5.25E+07 N·s·m	1.43E+06 Kg·m^2

3. SEISMIC ANALYSIS PROCEDURES

3.1 Modal Analysis

The basic vibration characteristics of the wind turbine system are first determined through modal analysis, where the Lanczos Block method was adopted. The comparisons of the natural frequencies of the wind turbine system with and without considering the SSI effect are given in Table 4. As shown in Figure 5, the first mode vibration is governed by flexural deformation of the tower along with the blades flap-wise motion (in X-Direction), and the second mode vibration is featured by the lateral bending vibration (in Y-Direction) of the tower along with the blades flap-wise motion. The third and fourth mode shapes mainly involve local vibration of the blades. The modal analysis results imply that a coupling model including the blades and tower should be adopted in the dynamic analysis of wind turbine systems in order to obtain accurate results. In general, the natural frequencies considering the SSI effect are smaller than the corresponding values without considering the SSI effect.

Table 4. Comparison of Frequencies of Models with &without Considering SSI Effect

Mode number	Frequency (Hz)		Difference /%
	Without considering SSI effect	Considering SSI effect	
1	0.345	0.328	2.27
2	0.402	0.380	3.43
3	0.411	0.403	1.95
4	0.425	0.410	3.53
5	0.994	0.971	2.31
6	1.472	1.342	8.83
7	2.032	1.353	33.3
8	2.063	1.362	33.9
9	2.446	1.381	43.4
10	2.502	1.417	43.3

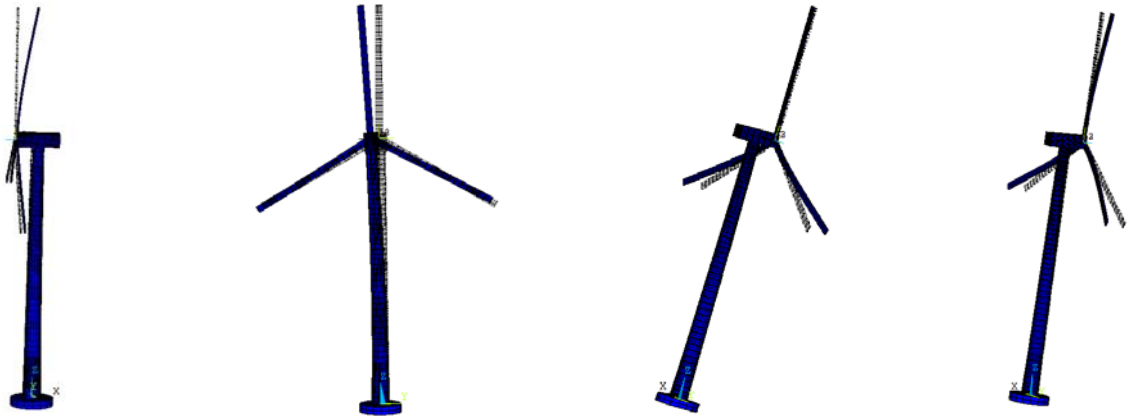

(a) (b) (c) (d)

Figure 5. The First Four Modal Shapes of the Wind Turbine Towers:
a) The first-order modal shape; b) The second-order modal shape;
c) The third-order modal shape; d) The fourth-order modal shape

3.2 Resonance Analysis

The purpose of performing resonance analysis is to avoid resonance when the tower is in operation. This requires that the structural natural frequencies should be sufficiently 'far away' from the external excitation frequency to ensure that structural dynamic response is within the controlled range. A common practice is that for wind turbine systems, all the natural frequencies f must stay away from the blade rotational frequency f_{1p} and blade passing frequency f_{np} (The subscript n is the number of blade), with the required differences larger than 10%. The number of the blade in this study is three, thus the blade-passing frequency f_{3p} is three times of the blade rotating frequency, namely, $f_{3p} = 3 f_{1p}$.

For the 1.25MW wind turbine system studied here, the working speed of the rotor is 9.6~17.8 r/min, and therefore the corresponding rotational frequency range is 0.16~0.29 Hz and the passing frequency range of the blade is 0.48~0.87 Hz. It is seen from Table 4 that these frequencies ranges stay away from the natural frequencies of the structure, and therefore, it can be concluded that no resonance will happen whether the SSI effect is taken into account or not. The comparisons of the natural frequencies against the rotating frequencies can also be done via the Campbell diagram shown in Figure 6.

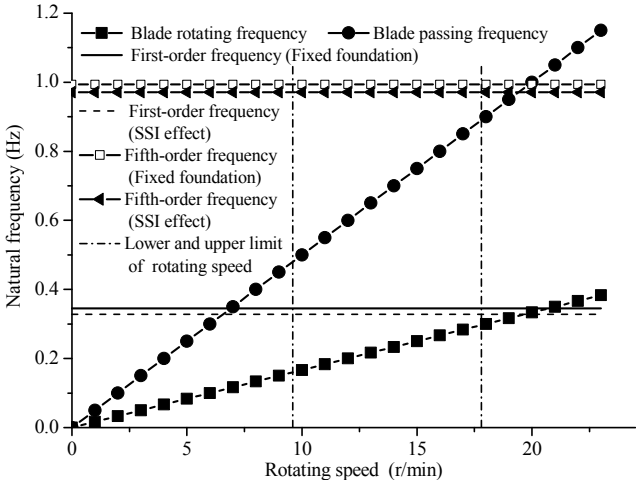

Figure 6. Campbell Diagram of Vibration in Wind Turbine System

3.3 Seismic Ground Motion Selection and Characteristic Comparisons

3.3.1 *Ground Motion Records Selection*

The EI-Centro (NS) wave, a typical bedrock wave which is widely used for seismic analysis, was chosen and two additional long-period seismic waves, namely, the HKD054 (EW) wave recorded in the Tokachi Oki earthquake in Japan in 2003 [20] and the CDAO (EW) wave recorded in the Mexico City of Mexico in 1985, were selected from the worldwide earthquake record database. The basic information of the three seismic waves is given in Table 5, and the acceleration time history curves of the three seismic waves are plotted in Figure 7. Hereafter, for ease of discussion, 'bedrock wave' stands for the EI-Centro (NS) wave, and the HKD054 (EW) wave and CDAO (EW) wave are referred as 'long-period waves'.

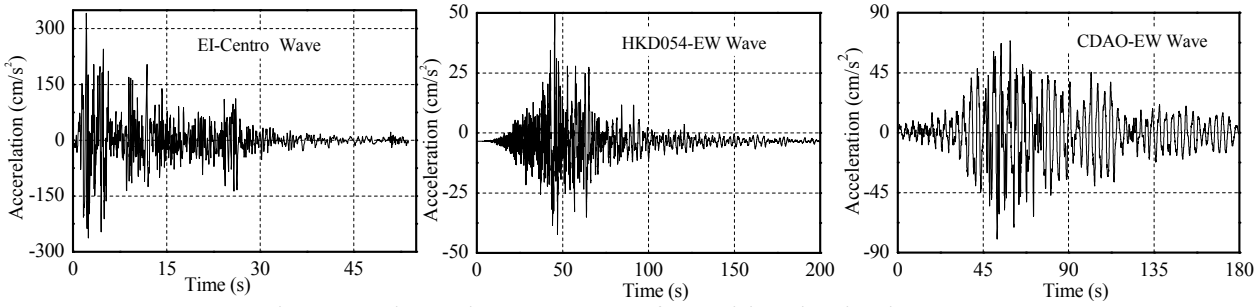

Figure 7. Time History Curves of Considered Seismic Waves

Table 5. Basic Information of Considered Seismic Waves

Earthquake wave	Magnitude	Date	Original record time (s)	Peak ground acceleration (gal)	Site classification
EI-Cento(NS)	6.4	6-Jun-1938	53.76	341.7	Ⅲ
HKD054(EW)	8.0	25-Sep-2003	213	50.53	Ⅳ
CDAO(EW)	8.1	19-Sep-1985	180	79.98	Ⅳ

It was considered that the site soil classification for the construction site of the wind turbine system is Ⅳ and the fortification intensity is Ⅶ [26]. For comparison purposes, the PGA of all the seismic waves was scaled to 35gal. For each seismic wave, three components were considered in the elastic time history analysis, and the accelerations along the horizontal principal direction (X-Direction), the lateral direction (Y-Direction) and the vertical direction were proportioned with the scaling coefficients of 1.0:0.85:0.65, respectively [26]. Raleigh damping was adopted in the structural model. The Rayleigh damping factor was calculated based on assigning 2% damping ratio to the first two modal frequencies. Due to the relatively long durations of the long-period seismic waves, a reduced duration of each wave was taken, starting from the time when 0.3PGA (peak ground acceleration) is first reached and ending when 0.3PGA last appears [33]. The main purpose of using reduced periods of seismic wave was to reduce the computational time, noting that the selected duration of seismic waves meets the relevant requirement for time history analysis [26]. No such reduction was made for the EI-Centro (NS) wave because the duration of the bedrock seismic waves is reasonably short. The time intervals and durations, for the analysis using, of the three seismic waves are illustrated in Table 6.

Table 6. Time Interval and Duration for Analysis of Considered Seismic Waves

Seismic Wave	EI-Centro(NS)	HKD054(EW)	CDAO(EW)
Time internal (s)	0.02	0.01	0.005
Duration (s)	53.76	42.20	79.72

Apart from the seismic excitation, gravity load and wind load were also taken into account in the analysis. It was assumed that the wind turbine system is in shutdown state when earthquake happens, and therefore the dynamic effect of rotating blade was not considered. The gust loading factor (GLF) method [34] was used to obtain the equivalent static wind load, i.e. mean wind load multiplied by a gust loading factor. It is worth mentioning that the gust-loading factor was obtained by a spectrum analysis method adopting the wind-induced random vibration theory along the wind direction. The calculated results of GLF and equivalent static wind load are detailed in Appendix A. In this study, the wind load was only applied in the X-direction, and therefore the modeling results obtained from the X-direction are used to reflect an extreme structural response where the maximum wind load and the earthquake occur concurrently. No wind load is applied in the Y-direction, and therefore the Y-direction response can be used to discuss the sole influences of earthquake characteristics. Multi-core parallel computing technology was adopted in the computing process.

3.3.2 *Basic Characteristics of Selected Ground Motions*

The frequency characteristics of the selected ground motion records can be shown with Fourier spectrums using the fast Fourier transform (FFT) method, as shown in Figure 8.

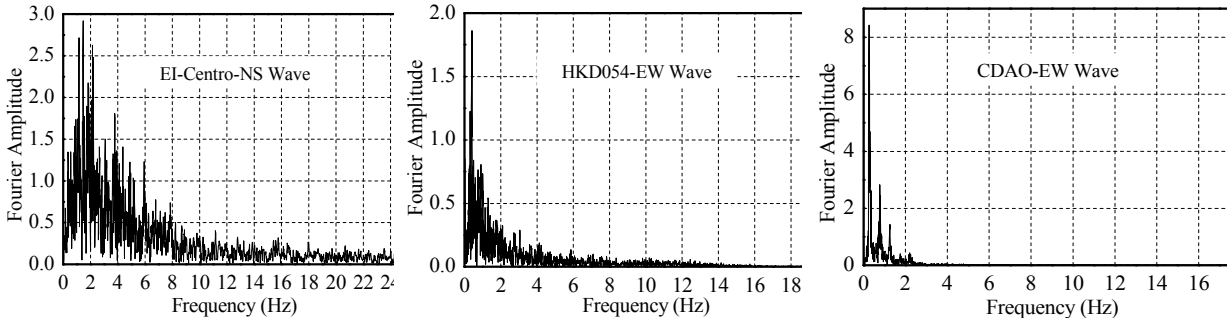

Figure 8. Fourier Frequency Spectrums

It can be seen that dominating frequency components are approximately distributed in 0.4-6 Hz for the EI-Centro (NS) wave. However, the dominating frequency ranges of the HKD054 (EW) and CDAO (EW) waves are approximately 0.2-1.3Hz and 0.22-0.8Hz, respectively. It is worth noting that the basis for determining the dominating frequency ranges for three seismic waves is that the ratio of area covered by the dominating frequency ranges to the total area of the Fourier amplitude spectrum reaches 80% in this study. Being different from the bedrock wave which involves significant high frequency components, the long-period waves are mainly governed by low frequency components. This may cause more significant seismic response for structures with long periods.

The response spectrums, as shown in Figure 9 in a normalized manner, can further reflect such dynamic characteristics of the selected seismic waves [22]. Here, the dynamic magnification factor is defined as the acceleration response spectrum normalized by the peak ground acceleration (PGA) value.

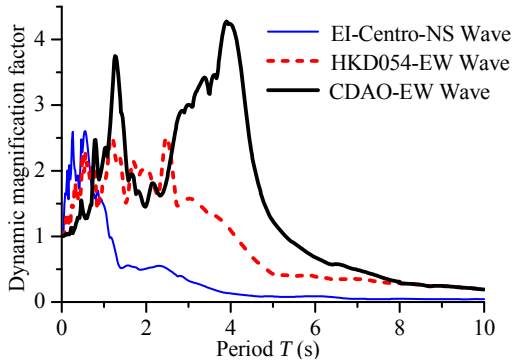

Figure 9. Acceleration Response Spectrums (ξ=0.02)

4. SEISMIC ANALYSIS RESULTS

4.1 Displacement Response

Considering both cases of fixed (rigid) foundation and that considering the SSI effect, the comparisons of the maximum height-wise displacements (in three directions) of the towers under the excitation of the bedrock and long-period seismic waves are shown in Figure 10. Some key response values are provided in Table 7. For ease of discussion, F model denotes the one with fixed (rigid) foundation, and S model refers to the one with 'elastic foundation', i.e. considering the SSI effect.

Table 7. Comparison of Maximum Displacements in Three Directions

Seismic Wave	The maximum displacement in X-Direction (mm)	The maximum displacement in Y-Direction (mm)	The maximum displacement in Z-Direction (mm)
EI-Centro-NS	890.36	25.53	32.01
HKD054-EW(F Model)	920.41	124.67	33.32
CDAO-EW(F Model)	984.14	65.64	35.76
HKD054-EW(S Model)	1170.95	111.72	38.46
CDAO-EW(S Model)	1239.53	147.31	40.89

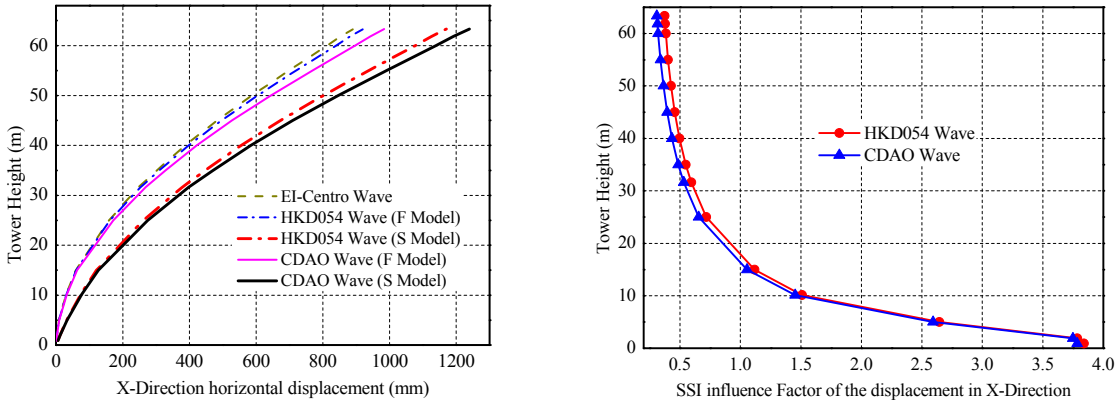

(a) (b)

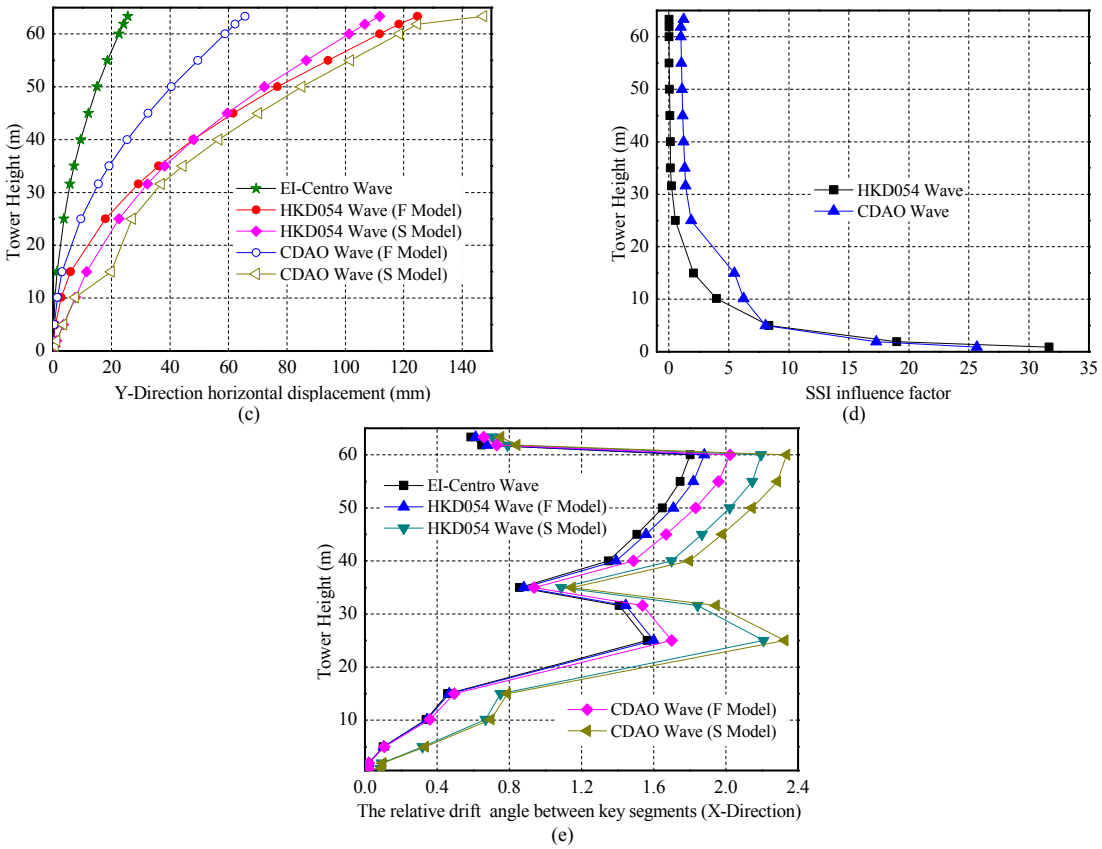

Figure 10. Nodal Displacement Analysis Results: a) Envelope Diagram of Horizontal Displacement in X-Direction; b) Variation of SSI Influence Factor (X-Direction); c) Envelope Diagram of Horizontal Displacement in Y-Direction; d) Variation of SSI Influence Factor (Y-Direction); e) Distribution of Drift Angle between Segments along Tower Height

It can be seen from Figure 10a and Figure 10c that with increase in height, the maximum nodal displacements in the two directions gradually increase, where the maximum displacement is observed at the tower top. Moreover, the displacement responses induced by the long-period seismic waves are obviously greater than the corresponding values caused by the bedrock seismic wave, especially at the top of the tower (see Table 7). Taking the deformation response along the Y-Direction for instance (F models), the maximum displacements induced by the long-period seismic waves can be 4.9 times of the corresponding values caused by the bedrock seismic wave. Due to the presence of the equivalent wind load applied along the X-Direction, the influence of the seismic wave types on the maximum nodal displacement in the X-Direction seems to be less pronounced. In general, the maximum top displacement (in X-Direction) under the combined wind and seismic action can reach nearly 1.0 m (see Figure 10a) when the tower is subjected to long-period seismic waves. Another issue that needs to be carefully addressed is the risk of pounding (between the blades and the tower) which can severely damage the entire wind turbine system (see Figure 11a), especially when the tower is in operation during an earthquake. Figure 11b and Figure 11c show the minimum gap between the blades and the tower during the considered earthquakes, taking account of the wind effect. It is clearly seen that the long-period waves lead to more noticeable vibrations of the blades and thus smaller minimum blade-tower gaps. In particular, HKD054 wave (F Model) leads to a minimum gap of -0.08 m, indicating that pounding would occur when the tower is hit by the considered wind and seismic loads. No such risk is observed for the case of bedrock wave.

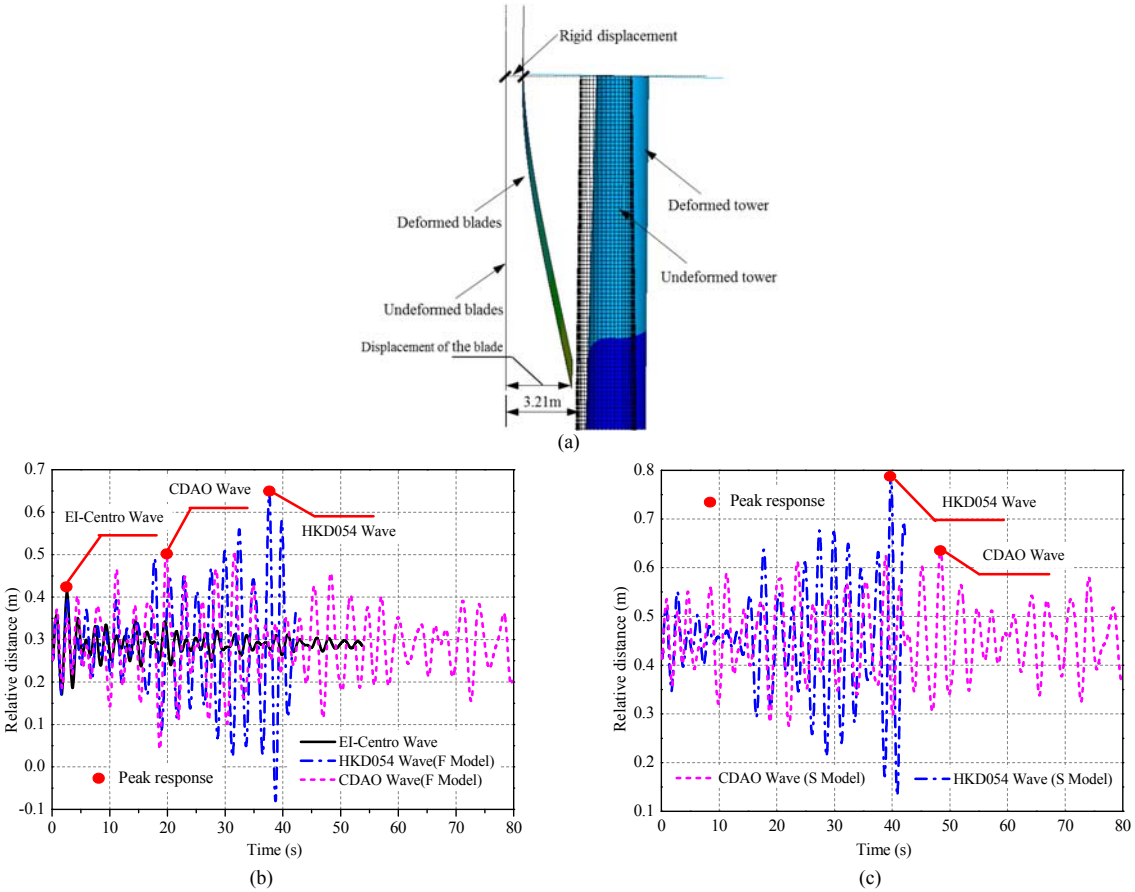

Figure 11. Relative Distance between the Blade Tip and the Tower: a) Illustration of Pounding between the Blades and the Tower; b) F Model Response; c) S Model Response

The displacement response is also affected by the SSI effect. In general, the nodal displacements of the towers including the SSI effect are larger than those without considering the SSI effect (see Figure 10a). When the SSI effect is considered, the maximum tower top displacement can achieve more than 1.2 m, corresponding to a drift level of approximately 2%. This drift level may cause failure of the foundation, leading to overturn of the tower. This effect should receive sufficient attention in future studies. In addition, the inclusion of the SSI effect may further exacerbate the influence of the long-period waves. As can be seen in Table 7, for the S-models, the maximum displacements induced by the long-period seismic waves can be 5.8 times that of the corresponding values caused by the bedrock seismic wave. This level of amplification is larger than that found in the F-models. This highlights the importance of considering the SSI effect for predicting the maximum deformation of the towers, especially when long-period seismic waves are considered. It is worth noting that the SSI effect seems to reduce the risk of pounding, as shown in Figure 11c. This is possibly due to the fact that the soil can help dissipate some input energy, leading to decreased vibration effect of the blades themselves. It is also of interest to see that some parts of the tower could have slightly decreased maximum deformation in Y-Direction when the SSI effect is included (under the HKD054-EW wave). This is because that the predominant frequency of the HKD054-EW record is closer to the second modal frequency of the F-model (compared with the S-model).

In order to more clearly show the influence of the SSI effect, a SSI influence factor, η, is defined by:

$$\eta = \frac{\text{Elastic foundation response value-Fixed foundation response value}}{\text{Fixed foundation response value}} \tag{4}$$

As indicated in Figure 10b and Figure 10d, for all the considered seismic waves, the influence of the SSI effect on the maximum nodal horizontal displacements at the lower part of the tower are significant. With increasing height, the influences of the SSI effect become less remarkable.

It can be observed in Figure 10e that the drift angle of key segments induced by the long-period waves are greater than the corresponding values for the case of bedrock wave, although a certain level of fluctuations can be observed. These fluctuations correspond to the stepped tube wall thickness variation locations as well as the locations where flexural stiffness change abruptly.

4.2 Acceleration Response

Apart from the displacement response, it is also necessary to investigate the acceleration response which may affect the functionality of electro-mechanical equipment. In this study, the structural acceleration response is presented by acceleration amplification coefficients, i.e. the ratio of maximum structural acceleration over the peak ground acceleration (PGA). The maximum acceleration amplification coefficients of the towers with and without considering the SSI effect are provided in Figure 12a through Figure 12c.

Table 8. Comparison of Maximum Acceleration Responses in Three Directions

Seismic Wave	The maximum acceleration in X-Direction (cm/s^2)	The maximum acceleration in Y-Direction (cm/s^2)	The maximum acceleration in Z-Direction (cm/s^2)
EI-Centro-NS	236.95	29.75	332.61
HKD054-EW(F Model)	275.66	88.36	614.02
CDAO-EW(F Model)	323.58	46.11	740.29
HKD054-EW(S Model)	268.38	64.86	612.66
CDAO-EW(S Model)	313.53	75.27	738.92

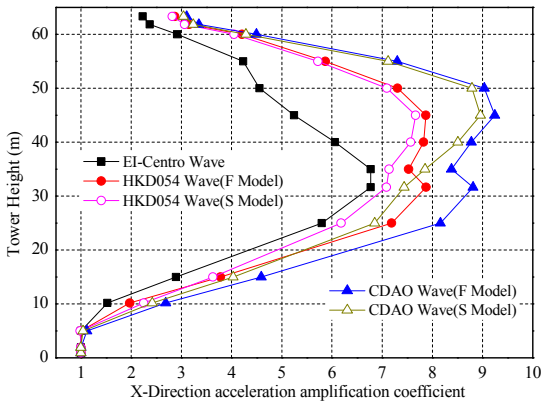

(a)

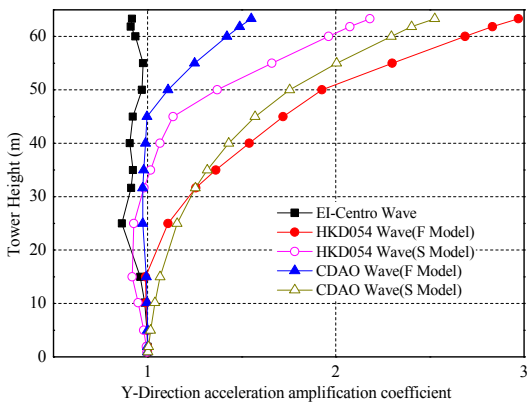

(b)

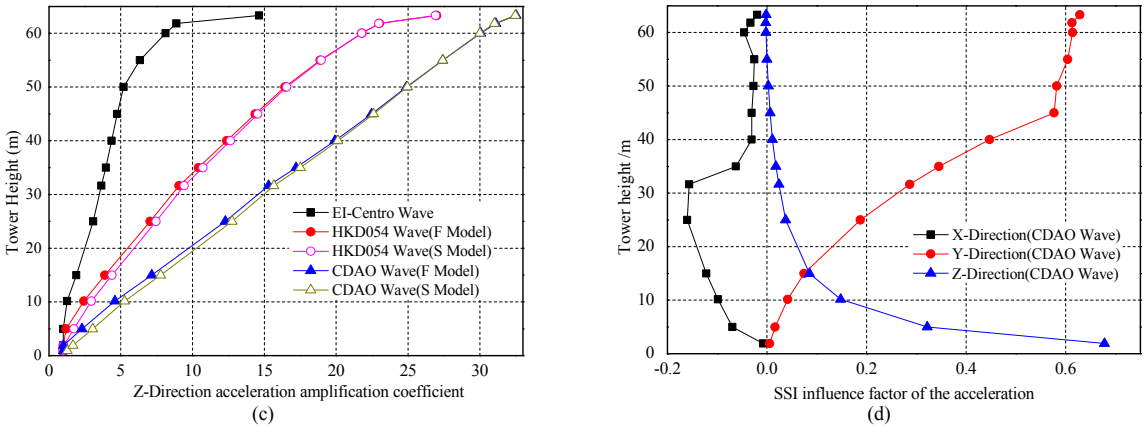

Figure 12. Acceleration Response Analysis Results: a) Envelope Diagram of Acceleration Amplification Coefficient (X-Direction); b) Envelope Diagram of Acceleration Amplification Coefficient (Y-Direction); c) Envelope Diagram of Acceleration Amplification Coefficient (Z-Direction); d) Variation of SSI Influence Factor (CDAO Wave)

It can be seen that the structural acceleration amplification coefficients induced by the long-period seismic waves are clearly larger than the corresponding values caused by the bedrock seismic wave, as detailed in Table 8. Taking the acceleration response along the Y-Direction for instance, the maximum acceleration response of the towers subjected to the long-period waves can be nearly 3 times that of the corresponding value for the case of the bedrock wave. In the X-Direction, at approximately 1/2-2/3 height of the tower, the acceleration amplification factor reaches its peak, and beyond this height the amplification coefficient starts to decrease. Similar behaviors were also reported by other researchers [15]. It is noted that at the top of the tower, the location of particular interest in terms of electric machine functionality, the maximum acceleration response (in the X-Direction) is not substantially increased when the long-period waves are considered instead of the bedrock wave. In the Y-Direction, the maximum acceleration response is slightly increased when the long-period waves are considered. This indicates that the maximum horizontal accelerations that the electric machines experience are not significantly influenced by the long-period waves. More attention needs to be paid for the acceleration in the vertical direction (i.e. Z-Direction), as the maximum height-wise accelerations in the Z-Direction increase apparently and the associated acceleration amplification is greater than those in the X and Y-Directions. At the top of the tower, the peak acceleration is 30 times more than the PGA under the long-period waves. This implies that the vertical earthquake action needs to receive sufficient attention in the design of wind turbine systems, especially when the tower is subjected to the long-period waves and the vertical acceleration at the tower top is of critical importance in design. Neglecting the vertical seismic action may lead to unsafe design.

The SSI effect tends to have inconsistent influence on the structural acceleration responses, as typically shown in Figure 12d. However, compared with the influence on nodal displacement (see Figure 10d), the influence of the SSI effect on acceleration is much less significant. Under certain conditions (e.g. HKD054-EW in X-Direction), the SSI effect tends to decrease the acceleration, and this is because that the soil could help dissipate some energy and thus to decrease the responses of the superstructure. It is noted that the maximum structural acceleration response is also affected by the relationship between the predominant frequency of the earthquake record and the critical modal frequencies of the structure, which explains the inconsistency of the SSI influence factors.

4.3 Stress Response

The height-wise maximum von Mises stresses (excluding the stress concentration effect near the door frame) of the tubular tower under the combined action of seismic load and wind load are shown in Figure 13a through Figure13c.

Table 9. Comparison of Height-wise Maximum Von Mises Stresses

Seismic Wave	The maximum von Mises stress (MPa)
EI-Centro-NS	209.77
HKD054-EW(F Model)	213.74
CDAO-EW (F Model)	226.65
HKD054-EW(S Model)	209.38
CDAO-EW (S Model)	224.47

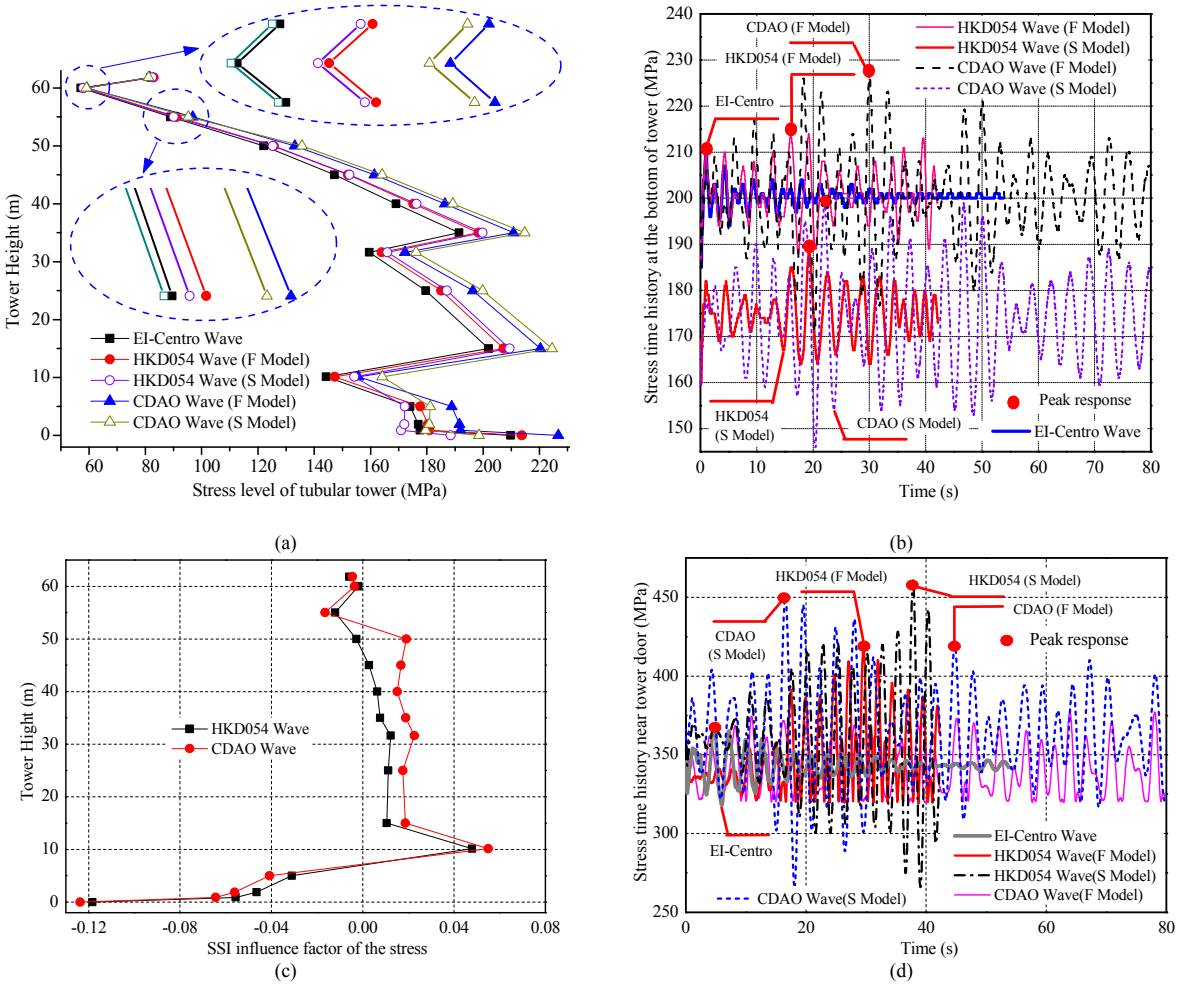

Figure 13. Stress Level Analysis Results: a) Stress Envelope Diagram of Tower along Height; b) Stress Time History at the Bottom of Tower; c) Variation of SSI Influence Factor on Stress; d) Stress Time History Near Tower Door

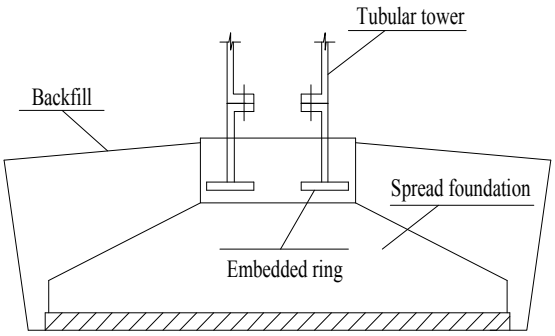

Figure 14. Typical Foundation of Wind Turbine Towers

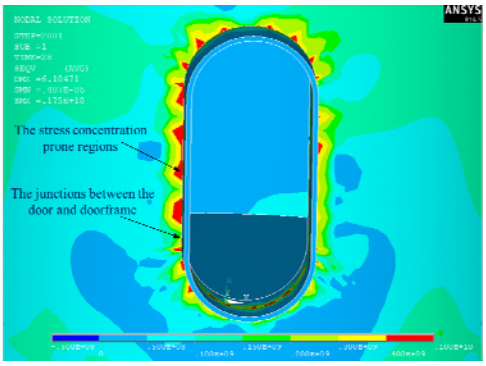

Figure 15. Stress Contour at the Junctions between Tower and Doorframe

Compared with the bedrock seismic wave, the long-period seismic waves could lead to higher stresses in the tower, as shown in Table 9.

In addition, as shown in Figure13a, compared with the case of fixed foundation, SSI effect could lead to slight decrease of the stress level near the foundation. As mentioned previously, this could be due to the extra energy dissipated by the surrounding soil. On the other hand, within the range between 15m and 50m of the tower height, the SSI effect can slightly increase the stress level. Moreover, with increase in height, the influence of the SSI effect on stress level decreases (see Figure 13c). In general, compared with the displacement and acceleration response, the influence of the SSI effect on stress response is much less significant.

For all the considered cases, the maximum von Mises stresses generally follow a decreasing trend with the increase of the tower height, although a certain level of fluctuations are observed. These fluctuations correspond to the stepped tube wall thickness variation locations as well as locations where the bending stiffness changes obviously. In general, the stress level along the height of the main body of the tower is within 230MPa, which is within the elastic range for normal constructional steel, and the stress distribution shows that the tapering design of the tower is quite economical in terms of material strength utilization.

Another important finding is that the local stress variation condition is more sensitive to the seismic waves and the SSI effect. The results given in Figure 13d show that the long-period waves could lead to increased level of stress concentration near the doorframe (see Figure 15). When the SSI effect is considered, the local stress near the doorframe is further increased, and the peak value could achieve nearly 460MPa. This indicates that the junctions between the tower and doorframe could experience significant stress concentration due to geometric discontinuity, and special attention needs to be paid to address this issue, especially when the long-period waves are considered.

4.4 Internal Forces

Based on the stress distributions, the internal forces, including base moment, base shear force, and axial force, of the tower can be extracted from the model.

Table 10. Comparison of Maximum Internal Force Responses

Seismic Wave	Shear force in X-Direction (kN)	Shear force in Y-Direction (kN)	Axial force in Z-Direction (kN)	Bending moment about X-axis (kN·m)	Bending moment about Y-axis (kN·m)	Torsion about Z-axis (kN·m)
EI-Centro	915.16	21.05	662.95	1107.51	44890.50	34.99
HKD054 (F Model)	928.64	91.74	924.32	5611.71	45761.25	125.35
CDAO (F Model)	976.68	52.77	1114.51	3012.01	48814.91	76.06
HKD054 (S Model)	927.27	64.50	933.81	3950.30	44142.22	137.20
CDAO (S Model)	971.31	80.50	1126.40	4750.53	46516.37	133.17

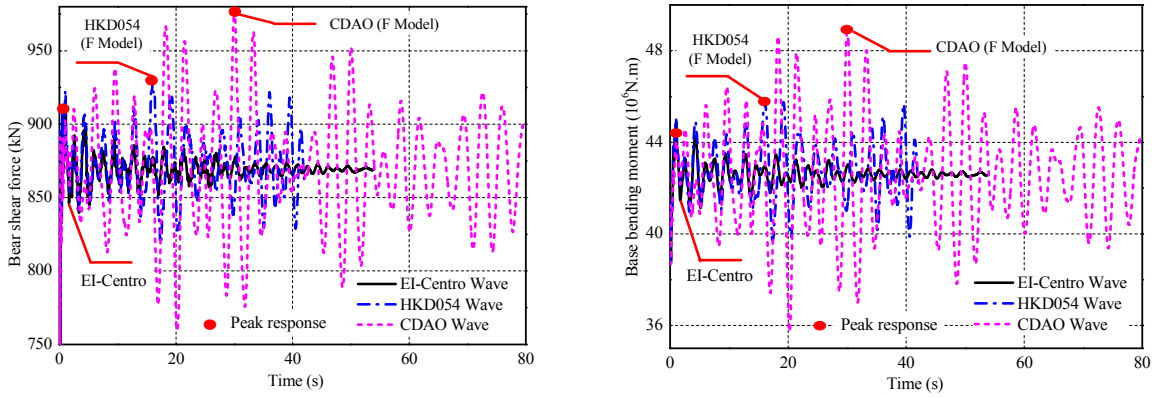

Figure 16. Base Internal Force Analysis Results: a) Base Shear Force Time History in X-Direction; b) Base Bending Moment Time History (about Y-axis)

Table 11. Comparison of spindle shear force responses

Seismic Wave	Shear force in Z-Direction (kN)	Shear force in Y-Direction (kN)	Resultant shear force (kN)
EI-Centro	634.24	14.28	634.41
HKD054(F Model)	781.07	67.33	783.97
CDAO(F Model)	864.15	35.85	864.89
HKD054(S Model)	797.56	47.09	798.95
CDAO(S Model)	884.15	57.29	886.01

According to Table 10 and Figure 16a through Figure 16b, the base shear forces, bending moments and torsions of the towers subjected to the long-period waves are greater than the results from the case of the bedrock wave. Taking the internal force responses along the Y-Direction for instance, the shear forces and bending moments (about X-axis) of the towers when subjected to the long-period waves are 2~5 times of the responses caused by the bedrock wave. It is noted that a similar degree of the increase in the displacement response is also observed. Due to the presence of the equivalent wind load applied along the X-Direction, the bending moment about Y-axis and the shear force along the X-Direction are quite significant. The combined moment and shear action may cause collapse of the towers if the foundation or the foundation embedded ring of the tower is not strong enough.

Another issue that needs to receive attention is the shear capacity of the spindle that links the blades to the nacelle (see Figure 3a). The vertical and horizontal vibrations of the tower in conjunction with the torsional effects could cause significant shear force at the spindle of the rotor. As can be seen in Table 11, the maximum shear force at the spindle generally exceeds 600 kN. The long-period seismic waves cause larger shear forces onto the spindle of the rotor, and the SSI effect could further increase this shear effect. It is worth mentioning that if the tower is in operation

during the earthquake, the rotating blades could cause an even larger dynamic shear force applied onto the spindle of the rotor. This cautions that if the shear force is too large, fracture of the spindle could happen.

5. PRELIMINARY DESIGN AND ANALYSIS ADVICE

Based on the information obtained from the finite element analysis, the fundamental seismic performances of the wind turbine tubular towers under long-period ground motions with the consideration of the SSI effect are understood, and some issues are also identified. Based on the research findings, some preliminary design comments are given as follows.

5.1 Door Frame

It can be seen from the analysis results that the junctions between the doorframe and tower door experience high stress levels (due to stress concentration). As a result, the weld of the doorframe may experience low-cycle fatigue failure during earthquakes and also potentially high-cycle fatigue failure under the wind action [35]. These areas may need to be strengthened locally if the tower is required to behave elastically during a design earthquake. Alternatively, an optimization study, examining the influences of varying geometric configurations of the door, may be performed to minimize the stress concentration effect near the doorframe. This is worth future investigations.

5.2 Foundations

The current study reveals that under a combined strong wind and seismic action, especially when the long-period waves are considered, considerably large displacement response can be induced at the top of the tower, noting that this is the location where the mass is concentrated. This displacement is further enlarged due to the SSI effect. This warns that overturn failure is a potential risk for towers located at soft soil regions. In recent years, the majority of the manufacturers adopt the embedded ring to connect the tubular tower and the foundation (see Figure 14). Although the peak stress for the current model is within the elastic range, a more severe earthquake may cause failure of the foundation, originating from the embedded ring. In fact, a number of overturn failures of such wind turbine towers have been reported [36]. Considering this, appropriate construction detailing may need to be applied to strengthen this “weak area”. To fix this problem, the recently developed prestressed-anchor foundation and prefabricated prestressed cylinder foundation, as shown in Figure 18, may be used, noting that the latter foundation form was specifically developed for soft soil regions.

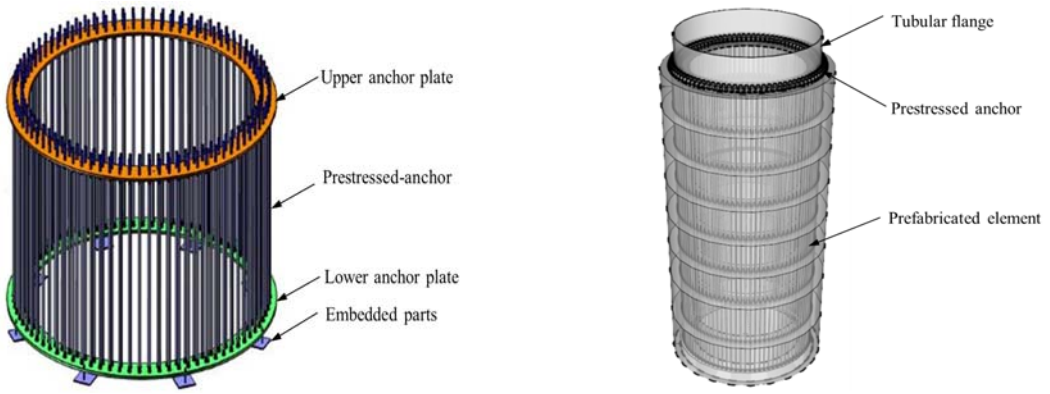

(a) A beam-slab prestressed-anchor foundation (b) A prefabricated prestressed cylinder foundation

Figure 18. New-type Foundation Forms for Wind Tubular Towers (http://www.goldenocean.cc/index.asp)

5.3 Ground Motion Selection and SSI Effect

Based on the current analysis results, SSI effect can amplify the structural responses (e.g. displacement, torsion effect, and axial force) under certain circumstances. With numerous wind turbine systems constructed in the soft soil regions, simplifying the foundation as a fixed constraint may be unsafe. In addition, the long-period seismic waves in the far field soft soil regions can also significantly increase the structural responses and the risk of pounding between the blades and the tower. In view of this, long-period seismic waves in conjunction with the SSI effect should be considered in the seismic design of the wind turbine systems in soft soil regions.

6. SUMMARY AND CONCLUSIONS

In this paper, an integrated finite element model consisting of rotor, nacelle, tower and foundation was established. To investigate the influence of long-period seismic waves and SSI effect on structural dynamic performances, two comparative models were built, and modal analysis, resonance analysis, and seismic time history analysis were conducted. Based on the numerical simulation results, the main conclusions are drawn as follows:

1) Considering the SSI effect can reduce the natural frequency of the wind turbine system. Therefore, the SSI effect should receive sufficient attention, especially when the towers are located in soft soil regions. Moreover, in order to capture some key responses including shear forces of the spindle and the risk of pounding, it is recommended that a coupling model including both the blades and tower is adopted in dynamic analysis of wind turbine towers.
2) The maximum displacement, acceleration, stress level and internal force responses of the tower subjected to the long-period seismic waves are significantly larger than the values obtained from the bedrock seismic wave. The long-period waves can also increase the risk of pounding between the blades and the tower. Therefore, long-period seismic waves are suggested to be considered in seismic design of such towers.
3) The influence of the SSI effect depends on a number of factors including the fundamental characteristic of the seismic wave and the modal frequencies of the tower itself. In general, the influences of the SSI effect on the maximum acceleration, stress level, and internal forces are not significant, whereas the maximum displacement response is much more sensitive to the SSI effect.
4) The acceleration amplification coefficients in the vertical direction are quite large, especially when the tower is subjected to long-period waves. As a result, neglecting the vertical seismic action

in seismic dynamic response analysis may lead to unsafe design, especially for electro-mechanical equipment functionality.

5) Adequate attention should be paid to the bottom part of the tower as well as the door regions. When the long-period waves are considered, the bending moment, shear force and von Mises stresses at the tower base section are apparently increased, and significant stress concentration effect can be observed near the doorframe. Appropriate strengthening approaches may be needed to decrease the stress demand at these critical locations, and thus to avoid extensive yielding as well as potential fatigue issues.

Finally, it is worth mentioning that the effect of the rotating blades is not considered in this paper. With the rotating blades disturbing the air flow, the wind field can be more complex. In future studies, a more accurate rotating wind speed spectrum model may be established for the dynamic response and fatigue analysis. Moreover, refined models should be established for the nacelle and flange plates to understand the dynamic response at these connection locations of the different components.

ACKNOWLEDGEMENTS

The authors wish to thank the Ministry of Science and Technology of China for financially supporting the research in the study through the Grant No. SLDRCE14-B-04. The authors would also like to thank Pacific Earthquake Engineering Research Center (PEER), National Research Institute for Earth Science and Disaster Prevention (NIED), Center for Engineering Strong Motion Data (CESMD) and U.S. Geological Survey (USGS) for their earthquake records provided.

REFERENCES

[1] Bilgili, M., Yasar, A. and Simsek, E., “Offshore Wind Power Development in Europe and its Comparison with Onshore Counterpart”, Renewable and Sustainable Energy Reviews, 2011, Vol.15, No.2, pp.905-915.

[2] Burton, T., Sharpe, D. and Jenkins, N., “Wind Energy Handbook”, New York: John Wiley & Sons, 2011, 2nd Section, pp. 1-7.

[3] Zhu, L., “Seismic Response of Wind Turbine in the Parked and Operating Conditions”, Departing of Civil Engineering, the University of Tokyo, Ph.D. Dissertation, 2007, pp.1-4.

[4] Lobitz, D. W., “A nastran-based Computer Program for Structural Dynamic Analysis of Horizontal Axis Wind Turbine”, Proceedings of the Horizontal Axis Wind Turbine Technology Workshop, Ohio, USA, 1984, Vol. 13, pp. 1-10.

[5] Bazeos, N., Hatzigeorgion, G. D., Hondros, I. D.,et al, “Static, Seismic and Stability Analyses of a Prototype Wind turbine Steel Tower”, Engineering Structures, 2002, Vol. 24, No. 8, pp. 1015-1025.

[6] Lavassas, I., Nikolaidis, G., Zervas, P., et al, “Analysis and Design of the Prototype of a Steel 1-MW Wind Turbine Tower”, Engineering Structures, 2003, Vol. 25, No. 8, pp. 1097-1106.

[7] Witcher, D., “Seismic Analysis of Wind Turbine in the Time Domain”, Wind Energy, 2005, Vol. 8, No.1, pp. 81-91.

[8] Murtagh, P. J., Collins, R., Basu, B., et al, “Dynamic Response and Vibration Control ofWind Turbine Towers”, Irish Engineers Journal, 2004, Vol. 58, No. 7, pp. 1-7.

[9] Murtagh, P. J., Basu, B. and Broderick, B. M., “Along-wind Response of a Wind Turbine Tower with Blade Coupling subjected to Rotationally Sampled Wind Loading”, Engineering Structures, 2005, Vol. 27, No. 8, pp. 1209-1219.

[10] Zhao, X. and Maißer, P., "Seismic Response Analysis of Wind Turbine Towers Including Soil-structure Interaction", Proceeding of the Institution of Mechanical Engineers, Part K: Journal of Multi-body Dynamics, 2006, Vol. 220,No. 1, pp.53-61.

[11] Zhao, X., Maißer, P. and Wu, J., "A New Multibody Modelling Methodology for Wind Turbine Structures using a Cardanic Joint Beam Element", Renewable Energy, 2007. Vol. 32, No. 3, pp. 532-546.

[12] Prowell ,I., Elgamal, A., Uang, C. and Jonkman, J., "Estimation of Seimic Load Demand for a Wind Turbine in the Time Domain", Proceeding of European Wind Energy Conference, Brussels, Belgium, 2010, Report No. NREL/CP 500, 47536.

[13] Díaz, O. and Suárez, L. E., "Seismic Analysis of Wind Turbines", Earthquake Spectra, 2014, Vol. 30, No. 2, pp. 743-765.

[14] Taddei, F. and Meskouris, K., "Seismic Analysis of Onshore Wind Turbine including Soil-structure Interaction Effects", Seismic Design of Industrial Facilities, 2014, pp. 511-522.

[15] Alati, N., Failla, G. and Arena, F., "Seismic Analysis of Offshore Wind Turbines on Bottom-fixed support Structures", Phil. Trans. R. Soc. A, 2015,Vol. 373, No. 2035, doi: 10.1098/rsta.2014.0086.

[16] Fang, C., Yam, M.C.H., Lam, A.C.C. and Xie, L., "Cyclic Performance of Extended End-plate Connections Equipped with Shape Memory Alloy Bolts", Journal of Constructional Steel Research, 2014, Vol. 94, pp. 122-136.

[17] Yam, M.C.H., Fang, C., Lam, A.C.C. and Zhang, Y.Y., "Numerical Study and Practical Design of Beam-to-column Connections with Shape Memory Alloys", Journal of Constructional Steel Research, 2015, Vol. 104, pp. 177-192.

[18] Karakalas, A.，Machairas, T.，Solomou, A.，Riziotis, V. and Saravanos, D., "Morphing Airfoil with Shape Memory Alloy Wire Actuators for Active Aerodynamic Load Control in Large Wind-Turbine Blades", EWEA 2015 Annual Event Conference, Paris, France, 2015.

[19] Yan, S., Yu, J. Y., Niu, J., and Wang, W., "Wind-induced Vibration Control of Wind Turbine Tower Structures based on Shape Memory Alloys", Journal of Disaster Prevention and Mitigation Engineering, 2016, Vol. 36, No. 1, pp. 159-164.

[20] Koketsu, K., Hatayama, K., Furumura, T., et al, "Damaging Long-period Ground Motions from the 2003 Mw 8.3 Tokachi-oki, Japan Earthquake", Seismological Research Letters, 2005, Vol. 76, No.1, pp. 67-73.

[21] Faccioli, E., Paolucci, R. and Rey, J., "Displacement Spectra for Long Periods", Earthquake Spectra, 2004, Vol. 20, No. 2 , pp. 347-376.

[22] Faccioli, E., Cauzzi, C., Paolucci, R., et al, "Long Period Strong Ground Motion and its Use as Input to Displacement Based Design", Earthquake Geotechnical Engineering, 2007, Vol. 6, pp. 23-51.

[23] Chung, Y. L., Nagae, T., Hitaka, T., et al, "Seismic Resistance Capacity of High-Rise Buildings Subjected to Long-Period Ground Motions: E-Defense Shaking Table Test", Journal of Structural Engineering, ASCE, 2012, Vol. 136, No. 6, doi:10.1061/(ASCE)ST.1943-541X.0000161.

[24] Ariga, T., Kanno, Y. and Takewaki, I., "Resonant Behaviour of Base-isolated High-Rise Building under Long-period Ground motions", The Structural Design of Tall and Special Buildings, 2005,Vol. 15,No. 3, pp. 325-338.

[25] BS EN 1998-1, "Eurocode 8: Design of Structures for Earthquake Resistance: Part 1: General Rules Seismic Actions and Rules for Buildings", Brussels: European Committee for Standardization, 2011.

[26] GB 50011-2010, "Code for Seismic Design of Buildings", Beijing: Ministry of Construction of the People's Republic of China, 2010.[in Chinese].

[27] ANSYS, Release 14.5, User's Manual, "Structural Analysis Guide", ANSYS Inc., 2012.

[28] Germanischer Lloyd (GL), “Guideline for the Certification of Wind Turbines: Part 5: Strength Analyses”, Hamburg, Germany, 2003.

[29] Wolf, J. P., “Spring-dashpot-mass models for foundationvibrations”, Journal of Earthqake Engineering and Structural Dynamics, 1997, Vol. 26, No. 9, pp. 931-949.

[30] Richart, F. E., Hall, J. R. and Woods, R. D., “Vibration of Soils and Foundations”, New York: Prentice-Hall, 1970, pp. 191-243.

[31] Ma, H.W., “Seismic Analysis for Wind Turbines including Soilstructure Interaction Combining Vertical and Horizontal Earthquake”, Proceedings of 15th World Conference on Earthquake Engineering, Lisbon, Portugal, 2012, pp. 336-345.

[32] Mulliken, J. S. and Karabalis, D.L., “ Discrete Model for Dynamic through-the-soil Coupling of 3-D Foundations and Structures”, Earthquake Engineering & Structural Dynamics, 1998, Vol. 27,No. 7, pp. 687-710.

[33] Watson, J. A. and Abrahamson, N. A., “Selection of Ground Motion Time Series and Limits on Scaling”, Soil Dynamics and Earthquake Engineering, 2006, Vol. 6 , No. 5, pp. 477-482.

[34] Davenport, A. G., “Gust Loading Factors”, Journal of the Structural Division, ASCE, 1967, Vol. 93, No.3, pp. 11-34.

[35] DIN EN 50308 Berichtigung 1 and VDE 0127-100 Berichtigung 1, “Wind Turbines-Protective Measures-Requirements for Design, Operation and Maintenance”, Berlin: Deutsches Institut für Normung, 2008.

[36] Agbayani, N. A., “Defects, Damage, and Repairs subject to High Cycle Fatigue: Examples from Wind Farm Tower Design”, Forensic Engineering Congress 2009: Pathology of the Built Environment, ASCE, 2009, pp. 546-555.

[37] GB 50009-2012, “Load Code for the Design of Building Structures”, Beijing: Ministry of Construction of the People’s Republic of China, 2012.[in Chinese].

Appendix A.

The calculated results of the gust loading factor (GLF) and the Equivalent static wind load

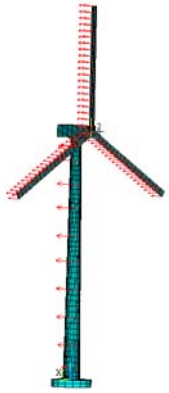

Figure 19. Wind Load on Wind Turbine Towers

According to the load code for the design of building structures [37], the basic wind pressure for the construction site of the wind turbine towers is 0.55 kN/m^2. In addition, the surface roughness classification is A. Moreover, the Simiu spectrum is adopted to obtain the wind-induced response in this study and the peak value factor is 2.2. Here, the blade parallel to the Z-axis is defined as blade 1, the other two blades are called blade 2 and blade 3 along the counter-clockwise direction. It is noted that the GLF values and the equivalent static wind load of the blade 2 are the same as those of the blade 3.

Table 12. GLF Value and Equivalent Static Wind Load of the Tower Body

Height (m)	3.32	9.95	16.59	23.22	29.89	36.50	43.13	49.76	56.40	59.72
GLF	2.114	2.128	2.141	2.153	2.165	2.177	2.191	2.204	2.221	2.238
the equivalent static wind load (kN)	31.256	39.243	42.643	44.342	45.069	45.137	44.752	43.973	42.903	42.429

Table 13. GLF Value and Equivalent Static Wind Load of the Blade 1

Height (m)	GLF	The equivalent static wind load (kN/m^2)
64.95	2.244	3.228
66.56	2.248	3.253
68.17	2.251	3.277
69.78	2.256	3.301
71.39	2.259	3.325
72.99	2.264	3.349
74.60	2.267	3.372
76.21	2.271	3.395
77.82	2.276	3.418
79.43	2.280	3.441
81.04	2.283	3.464
82.65	2.288	3.487
84.26	2.292	3.509
85.86	2.297	3.532
87.47	2.301	3.554
89.08	2.304	3.576
90.69	2.308	3.598
92.30	2.313	3.620
93.91	2.317	3.641
95.52	2.322	3.663

Table 14. GLF Value and Equivalent Static Wind Load of the Blade 2 and Blade 3

Height (m)	GLF	The equivalent static wind load (kN/m^2)
62.54	2.238	3.191
61.73	2.237	3.178
60.93	2.235	3.166
60.12	2.233	3.153
59.32	2.231	3.140
58.52	2.229	3.127
57.71	2.227	3.114
56.91	2.225	3.101
56.10	2.223	3.088
55.30	2.222	3.075
54.49	2.220	3.061
53.69	2.218	3.048
52.89	2.216	3.034
52.08	2.214	3.021
51.28	2.212	3.007
50.47	2.211	2.993
49.67	2.209	2.979
48.86	2.207	2.965
48.06	2.205	2.951
47.25	2.203	2.937